Submitted, Phil. Trans. of the Royal Society - A (2009)
http://www.cds.caltech.edu/~murray/papers/omm09-ptrs-a.html

Controlling biological networks by time-delayed signals

By Gábor Orosz[1,†], Jeff Moehlis[1] and Richard M. Murray[2]

[1]*Department of Mechanical Engineering, University of California, Santa Barbara, California, 93106, USA*
[2]*Control and Dynamical Systems, California Institute of Technology, Pasadena, California, 91125, USA*

This paper describes the use of time-delayed feedback to regulate the behavior of biological networks. The general ideas are demonstrated on specific transcriptional regulatory and neural networks. It is shown that robust yet tunable controllers can be constructed that provide the biological systems with model-engineered inputs. The results indicate that time delay modulation may serve as an efficient biocompatible control tool.

Keywords: time delay, control, gene regulatory network, neural network

1. Introduction

A common rule of thumb in engineering is that time delays can cause undesired oscillations. For example, the use of high frequency digital controllers (that introduce tiny delays into the control loops) can result in low frequency vibrations in robotic systems (Stépán [2001]). In most cases engineers are able to overcome these problems by using predictor algorithms (Mascolo [1999]). It may also occur that vibrations disappear for windows of larger delay where the efficiency of technological processes can even be higher (Dombovári *et al.* [2008]).

Recent papers have demonstrated that time delays can play important roles in biological systems. For example, in gene regulatory networks oscillations in protein levels may arise due to time delays (Monk [2003]; Novák & Tyson [2008]), and existing oscillations may become more robust (Stricker *et al.* [2008]; Ugander [2008]). Similarly, in neural networks delays may initiate different rhythmic spatiotemporal patterns (Coombes & Laing [2009]) and alter the stability of existing patterns (Ermentrout & Ko [2009]). Some works suggest that neural systems may even exploit time delays when encoding information into spatiotemporal codes (Kirst *et al.* [2009]; Orosz *et al.* [2009*a*]).

New interfaces allow us to interact with biological networks, i.e., to sense and regulate their behavior (Chalfie *et al.* [1994]; Sarpeshkar *et al.* [2008]; Popovych *et al.* [2006]). To design such regulators one needs to use techniques from control and dynamical systems theory (Åström & Murray [2008]). In this paper we demonstrate that tuning the time delays may provide us with additional 'degrees of freedom' for suppressing or changing the rhythmic behavior in biological systems. Broadly

† Author for correspondence (gabor@engineering.ucsb.edu).

speaking, besides varying the strength of the control actions (i.e., the gains) one may also modulate the timing of the actions by varying the delays. Such a strategy is usually avoided in engineering systems since it requires the use of delay differential equations and infinite dimensional phase spaces. On the other hand, exploiting the richness of such dynamics may prove to be beneficial when interacting with living organisms.

We demonstrate these ideas in two different biological networks. In Sec. 2 we consider a simple synthetic gene regulatory circuit, called the repressilator. We show that one may stabilize the steady state of protein expression by using an additional regulatory gene with appropriate time delays. In Sec. 3 a simple neural network is studied. Based on the stability analysis of oscillatory solutions we construct an event-based act-and-wait type of controller that uses delayed inputs to drive the systems into a chosen oscillatory state. Finally, in Sec. 4 we conclude our results and discuss future research directions.

2. Controlling equilibria in gene regulatory networks

Intracellular spaces are filled with biochemical regulatory networks in every organism. In particular, gene regulatory networks allow cells to express proteins when needed (Bolouri [2008]; Courey [2008]). Genes (sections of DNA) are transcribed into mRNA (by RNA polymerase) and then mRNA is translated into proteins (by ribosomes). The resulting proteins go through configurational changes (called folding) in order to become 'biochemically active'. An active protein then may bind to the so-called promoter region of another gene and activate or repress the transcription of the corresponding gene (and in turn regulate the expression of the corresponding protein). Indeed, both transcription and translation takes a finite amount of time that introduce time delays into the modelling equations (Monk [2003]; Novák & Tyson [2008]).

Due to the large number of genes in living cells it is very difficult to map out the dynamics of natural gene regulatory networks. For this reason, a different approach has been initiated about a decade ago when the first synthetic transcriptional regulatory circuits were constructed and implanted into living cells; see (Elowitz & Leibler [2000]) for the repressilator and (Gardner *et al.* [2000]) for the toggle switch. Using fluorescent proteins as output signals the dynamics of synthetic circuits can be studied in detail (Chalfie *et al.* [1994]).

Gene regulatory networks can exhibit robust oscillatory behavior. For example, circadian rhythms in cells are driven by such genetic oscillations (Dunlap [1999]). On the other hand, mutant genes may lead to pathological oscillations (Novák & Tyson [2008]). One way to suppress such oscillations might be to implant extra regulatory genes into the cells. One can design where to 'take a signal out' by implanting a gene that is repressed or activated by a chosen protein of the system. It is also possible to 'insert a signal' by using a protein that activates or represses a chosen gene in the system. However, in order to stabilize an equilibrium without changing it (i.e., without changing the steady state values of mRNA and protein concentrations), the gains need to satisfy extra constraints. These constraints may still allow stabilization if additional time delays are built into the controller. Note that transcriptional delays may be increased by inserting 'junk' sections into the gene and translational delays can be enlarged by slowing down the protein fold-

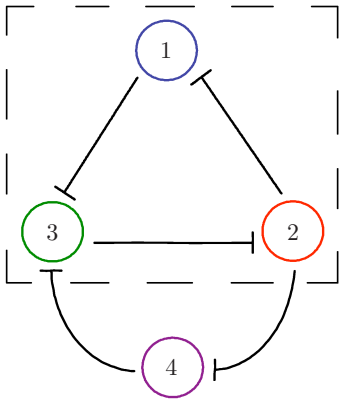

Figure 1. Sketch of the repressilator (subnetwork marked by the dashed frame) with and additional regulatory gene attached.

ing; see (Ugander [2008]) for more details on delay engineering in transcriptional regulatory networks.

Here we test these ideas on the repressilator that consists of three genes coupled to each other to form a unidirectional ring as depicted by the subnetwork within the dashed frame in Fig. 1. Each circle represents a gene and its protein product (Elowitz & Leibler [2000]). This circuit shows robust oscillatory behavior in wide regions of parameters. It was shown that increasing the transcriptional and translational delays between the repressilator elements 1,2,3 leads to more robust oscillations, i.e., they appear in more extended parameter domains and become more attractive (Chen & Aihara [2002]; Ugander [2008]). On the other hand, we show that by attaching an additional element and choosing the corresponding delays appropriately the oscillations can be suppressed: see the extra regulatory element 4 outside the dashed frame in Fig. 1.

The regulated system can be modelled by the delay differential equations

$$\begin{aligned}
&\dot{m}_i(t) = -m_i(t) + \alpha\, f\big(p_{i+1}(t)\big)\,, \\
&\dot{p}_i(t) = -\beta\, p_i(t) + \beta\, m_i(t)\,, \qquad\qquad i = 1, 2\,, \\
&\dot{m}_3(t) = -m_3(t) + \alpha\, f\big((1-\eta)p_1(t) + \eta\, p_4(t)\big)\,, \\
&\dot{p}_3(t) = -\beta\, p_3(t) + \beta\, m_3(t)\,, \\
&\dot{m}_4(t) = -m_4(t) + \alpha\, f\big(p_2(t-\sigma)\big)\,, \\
&\dot{p}_4(t) = -\beta\, p_4(t) + \beta\, m_4(t-\tau)\,,
\end{aligned} \tag{2.1}$$

where each gene is repressed through the nonlinear function

$$f(p) = \frac{1}{1+p^n} + f_0\,, \tag{2.2}$$

that is depicted by the decreasing curve in Fig. 2. Here the dot represents the derivative with respect to time t and $m_i, p_i \geq 0$ are the concentrations of mRNA and protein for the i-th species. For the sake of simplicity, parameters are chosen to be identical for each gene-protein pair. We assume that the time delays are small

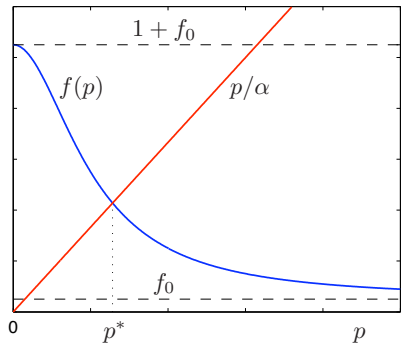

Figure 2. Finding the equilibrium value p^* of protein concentration. The increasing straight line and the decreasing curve correspond to the left and right sides of the algebraic equation (2.4) where f is given by (2.2).

in the original system (these are set to zero for $i = 1, 2, 3$), but the extra regulatory element contains significant transcriptional and translational delays (denoted by σ and τ, respectively). The time is measured in units of mRNA degradation time, the protein concentrations are rescaled by the number of proteins needed to half-maximally repress a gene, and the mRNA concentrations are rescaled by the number of proteins expressed per mRNA molecule in steady state. The rescaled parameters α and β represent the strength of the repression and the protein degradation rate, respectively, and these can be determined from dimensional parameters. In this paper we consider the 'leakage constant' $f_0 = 10^{-3}$ and the Hill coefficient $n = 2$, for which oscillations appear in a wide ranges of parameters α, β. We recall that $\alpha = 215.52, \beta = 0.2069$ were used in (Elowitz & Leibler [2000]) where oscillations were demonstrated experimentally.

We assume that there is only one binding site at the promoter region of a gene, that is, in case of gene 3 either protein p_1 or protein p_4 binds but not both; see Fig. 1. More precisely, we assume that p_4 binds with probability $\eta \in [0, 1]$ and so p_1 binds with probability $(1-\eta)$ as expressed in the last term of the equation for $\dot{m}_3$ in (2.1). Notice that when choosing $\eta = 0$ the repressilator with genes $1, 2, 3$ is obtained, while for $\eta = 1$ another repressilator emerges with genes $2, 3, 4$ and time delays σ and τ. In both of these special cases oscillations occur due to unstable equilibria. As will be shown below these oscillations may be suppressed for certain intermediate values of η by choosing the delays appropriately. We note that one may model competitive binding by using the nonlinear combination $\eta_1 f\big(p_1(t)\big) + \eta_4 f\big(p_4(t)\big)$ with $\eta_1, \eta_4 \geq 0$ instead of $f\big((1-\eta)p_1(t) + \eta\, p_4(t)\big)$ in the equation for $\dot{m}_3$ in (2.1). The linear stability diagrams obtained in this case are qualitatively similar to those presented in this paper. We also remark that there exist genes with multiple binding sites and one may use the resulting combinatorial features when designing genetic controllers (Cox *et al.* [2007]).

System (2.1) possesses the 'symmetric' equilibrium

$$m_i(t) \equiv p_i(t) \equiv p^*\,, \tag{2.3}$$

for $i = 1, 2, 3, 4$ where p^* is the unique solution of

$$p/\alpha = f(p)\,, \tag{2.4}$$

as demonstrated in Fig. 2. Note that $p^* = p^*(\alpha, f_0, n)$ and p^* is monotonically increasing in α. Also notice that (2.4) is independent of η, σ and τ, that is, the extra regulatory gene does not change the equilibrium of the systems. This occurs since the parameters α and β for the extra element 4 are considered to be identical to the parameters for the original system 1,2,3. Modulating these parameters (in the last two equations in (2.1) only) may suppress the oscillations but it destroys the symmetry and so changes the equilibrium. Contrarily, varying η, σ and τ may allow us to stabilize the equilibrium without altering it.

Let us define the perturbations

$$\begin{aligned} a_i(t) &:= m_i(t) - p^*\,, \\ b_i(t) &:= p_i(t) - p^*\,, \end{aligned} \tag{2.5}$$

and introduce the vector notation

$$\begin{aligned} \mathbf{a} &= \begin{bmatrix} a_1 & a_2 & a_3 & a_4 \end{bmatrix}^T\,, \\ \mathbf{b} &= \begin{bmatrix} b_1 & b_2 & b_3 & b_4 \end{bmatrix}^T\,. \end{aligned} \tag{2.6}$$

Thus, the linearization of (2.1) about (2.3) can be written as

$$\begin{bmatrix} \dot{\mathbf{a}}(t) \\ \dot{\mathbf{b}}(t) \end{bmatrix} = \begin{bmatrix} -\mathbf{I} & \alpha\kappa\mathbf{A_0} \\ \beta\mathbf{B_0} & -\beta\mathbf{I} \end{bmatrix} \begin{bmatrix} \mathbf{a}(t) \\ \mathbf{b}(t) \end{bmatrix} + \begin{bmatrix} \mathbf{O} & \alpha\kappa\mathbf{A}_\sigma \\ \mathbf{O} & \mathbf{O} \end{bmatrix} \begin{bmatrix} \mathbf{a}(t-\sigma) \\ \mathbf{b}(t-\sigma) \end{bmatrix} + \begin{bmatrix} \mathbf{O} & \mathbf{O} \\ \beta\mathbf{B}_\tau & \mathbf{O} \end{bmatrix} \begin{bmatrix} \mathbf{a}(t-\tau) \\ \mathbf{b}(t-\tau) \end{bmatrix}\,, \tag{2.7}$$

where

$$\begin{aligned} \mathbf{A_0} &= \begin{bmatrix} 0 & 1 & 0 & 0 \\ 0 & 0 & 1 & 0 \\ 1-\eta & 0 & 0 & \eta \\ 0 & 0 & 0 & 0 \end{bmatrix}\,, \quad \mathbf{A}_\sigma = \begin{bmatrix} 0 & 0 & 0 & 0 \\ 0 & 0 & 0 & 0 \\ 0 & 0 & 0 & 0 \\ 0 & 1 & 0 & 0 \end{bmatrix}\,, \\ \mathbf{B_0} &= \begin{bmatrix} 1 & 0 & 0 & 0 \\ 0 & 1 & 0 & 0 \\ 0 & 0 & 1 & 0 \\ 0 & 0 & 0 & 0 \end{bmatrix}\,, \qquad \mathbf{B}_\tau = \begin{bmatrix} 0 & 0 & 0 & 0 \\ 0 & 0 & 0 & 0 \\ 0 & 0 & 0 & 0 \\ 0 & 0 & 0 & 1 \end{bmatrix}\,, \end{aligned} \tag{2.8}$$

$\mathbf{I}$ and $\mathbf{O}$ denotes the 4×4 identity and zero matrices, respectively, and

$$\kappa = f'(p^*) < 0\,. \tag{2.9}$$

Note that $p^* = p^*(\alpha, f_0, n)$ implies $\kappa = \kappa(\alpha, f_0, n)$.

Now considering the trial solution $\mathbf{a}(t) = \bar{\mathbf{a}}\,\mathrm{e}^{\lambda t}$, $\mathbf{b}(t) = \bar{\mathbf{b}}\,\mathrm{e}^{\lambda t}$ with constant vectors $\bar{\mathbf{a}}, \bar{\mathbf{b}} \in \mathbb{R}^4$ and eigenvalues $\lambda \in \mathbb{C}$, the characteristic equation

$$\begin{aligned} D(\lambda) &= \det \begin{bmatrix} (\lambda+1)\mathbf{I} & -\alpha\kappa\big(\mathbf{A_0} + \mathbf{A}_\sigma \mathrm{e}^{-\lambda\sigma}\big) \\ -\beta\big(\mathbf{B_0} + \mathbf{B}_\tau \mathrm{e}^{-\lambda\tau}\big) & (\lambda+\beta)\mathbf{I} \end{bmatrix} \\ &= (\lambda+1)(\lambda+\beta)\Big\{(\lambda+1)^3(\lambda+\beta)^3 - (\alpha\beta\kappa)^3\big(1-\eta+\eta\,\mathrm{e}^{-\lambda(\sigma+\tau)}\big)\Big\} = 0 \end{aligned} \tag{2.10}$$

is obtained. This equation has infinitely many solutions for the eigenvalues λ in correspondence to the infinite dimensional phase space of (2.1) and (2.7). The equilibrium (2.3) is asymptotically stable if and only if all eigenvalues lie in the left-half complex plane. When varying the parameters, the equilibrium may lose its stability via Hopf bifurcation if a pair of complex conjugate eigenvalues crosses the imaginary axis. This bifurcation results in periodic oscillations. To determine the stability boundaries we substitute $\lambda = \mathrm{i}\omega$, $\omega \in \mathbb{R}^+$ into (2.10), separate the real and imaginary parts and apply some trigonometric identities. The stability curves in the $(\sigma+\tau, \eta)$ parameter plane are given by

$$\begin{aligned} \sigma+\tau &= \frac{1}{\omega}\left\{ \pm \operatorname{Arccos}\left(\frac{c_1^2-c_2^2-2c_1+1}{c_1^2+c_2^2-2c_1+1}\right) + (2\ell+1)\pi \right\}, \quad \ell = 0,1,2,\dots \\ \eta &= \frac{c_1^2+c_2^2-2c_1+1}{-2c_1+2}, \end{aligned} \tag{2.11}$$

where

$$\begin{aligned} c_1 &= \frac{(\beta-\omega^2)\big((\beta-\omega^2)^2-3(1+\beta)^2\omega^2\big)}{(\alpha\beta\kappa)^3}, \\ c_2 &= \frac{(1+\beta)\omega\big(3(\beta-\omega^2)^2-(1+\beta)^2\omega^2\big)}{(\alpha\beta\kappa)^3}, \end{aligned} \tag{2.12}$$

and the $+$ and $-$ signs are considered when $\sin(\omega(\sigma+\tau)) < 0$ and $\sin(\omega(\sigma+\tau)) > 0$, respectively.

The curves for $\ell = 0$ are plotted in Fig. 3 for different values of α and β; the original repressilator parameters are used in panel (a). The curves for $\ell > 0$ appear for larger delays to the right of the $\ell = 0$ curves and these are out of the window. Using infinite dimensional generalizations of the Routh-Hurwitz criteria (Stépán [1989]), one may determine that the steady state is linearly stable in the shaded domain. Notice that when decreasing or increasing α [panels (a,b,c)] the stable regime does not change significantly, only becoming a bit more extended corresponding to the fact that oscillations appear to be most robust for intermediate values of α in the uncontrolled repressilator (Elowitz & Leibler [2000]). On the other hand, the stable domain shrinks and moves closer to the vertical axis when decreasing β [panels (a,d,e)].

When a stability curve crosses itself a codimension-two Hopf bifurcation occurs, i.e., two pairs of complex conjugate eigenvalues cross the imaginary axis that leads to quasiperiodic oscillations. We remark that such bifurcations occur rarely in dynamical systems without delay but they are quite typical in delayed systems (Stépán [1989]). Note that the equilibrium may lose its stability via fold bifurcation when a real eigenvalue crosses the imaginary axis due to parameter variations. This cannot occur here for $\sigma = \tau = 0$ since $\kappa = f'(p^*) < 0$. Consequently, it cannot occur for any $\sigma, \tau > 0$ as can be seen by substituting $\lambda = 0$ into (2.10). We also remark that incorporating the time delays in the interactions between the repressilator genes 1,2,3 the stability regimes can still be determined, however, the calculations become more elaborate and so less instructive.

In Fig. 3(b) we marked the points A and B and the corresponding numerical simulation results are shown in Fig. 4(a) and (b), respectively. In both cases the

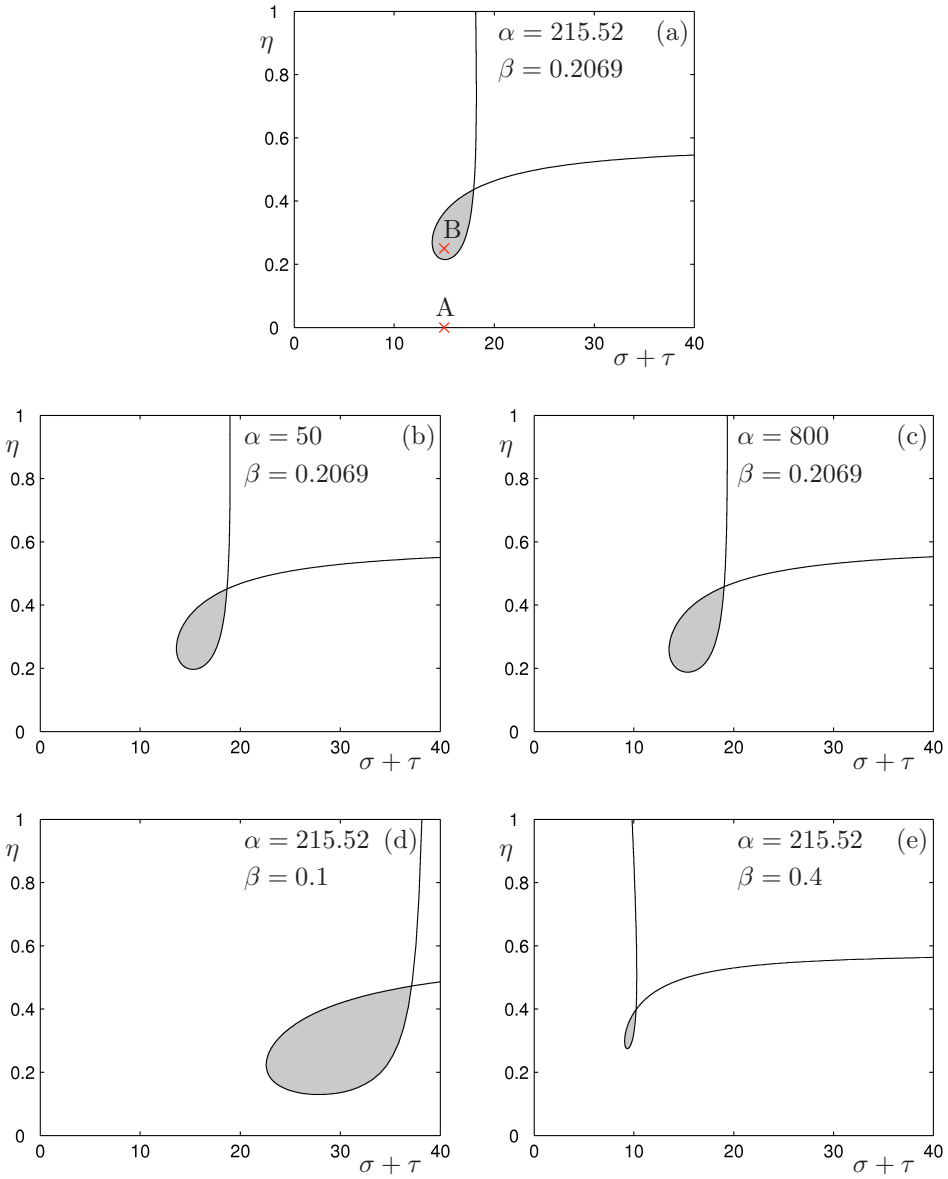

Figure 3. Stability diagrams for the controlled repressilator for different repression strengths α and protein degradation rates β. The equilibrium (2.3) is linearly stable in the shaded domains. Points A and B in panel (a) correspond the simulations shown in Fig. 4(a) and (b), respectively.

same initial conditions are chosen. Recall that the initial conditions for delay differential equations are functions in the delay interval $t \in [-\max\{\sigma, \tau\}, 0]$, that are chosen to be constant functions here. When the equilibrium is unstable (point A in Fig. 3(b) at $\sigma+\tau = 15, \eta = 0$), oscillations arise. The time profiles for the repressilator protein concentrations p_1, p_2, p_3 are displayed in the top panel of Fig. 4(a). The

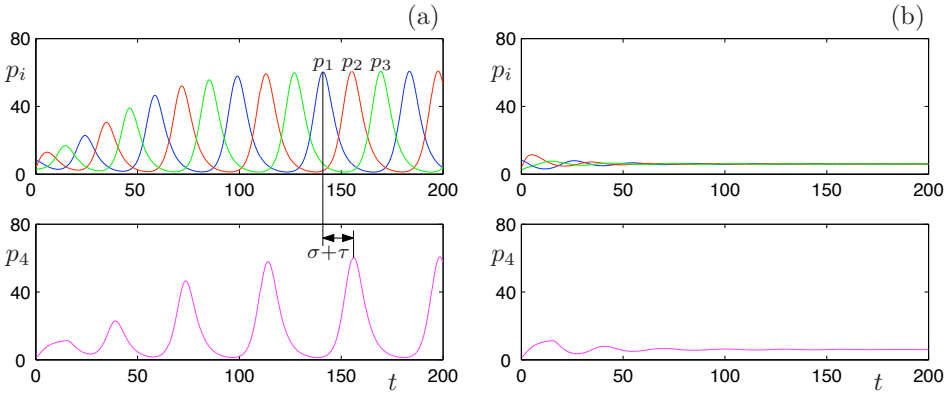

Figure 4. Demonstrating the action of the genetic controller by numerical simulations. The protein concentrations p_1, p_2, p_3 for the repressilator are shown on the top and the protein concentration p_4 for the extra regulatory gene is displayed at the bottom. Panels (a) and (b) correspond to the points A and B in Fig. 3(a).

system approaches a travelling wave solution where the time profile of the $(i+1)$-st protein can be obtained by shifting the time profile of i-th protein by $T_{\rm p}/3$ where $T_{\rm p}$ is the period of oscillations. This pattern corresponds to the Z_3 discrete rotational symmetry in the system and may also be interpreted as a splay state since the concentration of each protein 'fires' separately and equidistantly in time. The time evolution for the protein concentration p_4 is shown in the bottom panel in Fig. 4(a). Since $\eta = 0$ and p_1 and p_4 are both driven by p_2, the time profiles for p_4 can be obtained by shifting the p_1 signal with $\sigma+\tau$. When the equilibrium is stable (point B in Fig. 3(b) at $\sigma + \tau = 15, \eta = 0.25$), no oscillations develop as shown in Fig. 4(b). This demonstrates that the equilibrium can be stabilized by tuning the aggregated delay $\sigma + \tau$ and the binding probability η .

We note that one may find oscillations even for a stable equilibrium when considering certain specific initial conditions. This suggests that the Hopf bifurcations may be subcritical. It may be and interesting future research to map out bifurcation structure for the arising periodic solutions but that is beyond the scope of this paper. In the next section however we investigate a time-delayed network where it is essential to study the stability of oscillatory solutions. Such investigations allow us to construct a controller that can stabilize a chosen rhythm.

3. Controlling periodic solutions in neural networks

Oscillations are ubiquitous in neural networks: rhythmic patterns of electric activity are used to represent information about the environment and about the state of the animal in many different ways (Rabinovich *et al.* [2006]). However, some of these rhythms, for example, full synchrony, may be pathological and lead to macroscopic tremors like in Parkinson's disease. (In contrast, in technological systems full synchrony is often desired (Olfati-Saber & Murray [2004]).)

One way to avoid these harmful oscillations (without destroying all rhythms) might be to inject weak external current into specific brain areas. For example, when injecting different signals at multiple sites, neurons may entrain their rhythms to

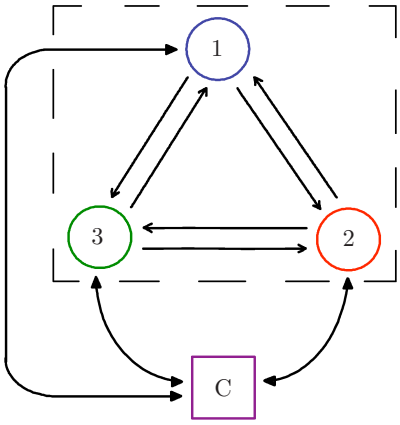

Figure 5. Sketch of a network of 3 globally coupled neurons (subnetwork marked by the dashed frame) with a controller attached.

the signal of the nearby electrode and so the overall synchrony can be destroyed (Popovych *et al.* [2006]). However, this control strategy may force the neural system into an 'artificial state'. Instead, one may select a natural rhythm and try to stabilize it. Since neurons communicate with electric signals (called spikes), it takes a considerable amount of time to transmit the signal from one neuron to another. Consequently, time delays appear in the modelling equations. When varying the delays different stable patterns (e.g., full synchrony, clustering) can emerge (Ermentrout & Ko [2009]). As will be shown below one may construct a controller that mimics the delayed interactions of neurons and so drives the system away from synchrony into a chosen cluster state.

We demonstrate these ideas in a simple system of three neurons with all-to-all coupling as depicted inside the dashed frame in Fig. 5. We assume that the voltage of each neuron can be measured and current can be injected into each cell; see the controller C outside the dashed frame in Fig. 5. To describe the activity of the somas we use the Hudgkin-Huxley model which models the cell membrane as a simple electric circuit (Hodgkin & Huxley [1952]). We consider direct electrotonic couplings (gap junctions) between the neurons and incorporate axonal delays to model the time required to transmit the signal along the axons between the neurons. For simplicity, we omit dendritic delays (associated with signal transmission along dendrites) and synaptic delays (the time needed to release chemicals in synapses); see (Campbell [2007]; Ermentrout & Ko [2009]) for more details on these effects.

The time evolution of the controlled system is given by the delay differential

equations

$$\begin{aligned}
\dot{V}_i(t) &= \frac{1}{C}\Big(I - g_{\mathrm{Na}} m_i^3(t) h_i(t)\big(V_i(t) - V_{\mathrm{Na}}\big) - g_{\mathrm{K}} n_i^4(t)\big(V_i(t) - V_{\mathrm{K}}\big) - g_{\mathrm{L}}\big(V_i(t) - V_{\mathrm{L}}\big) \\
&\qquad + \varepsilon \sum_{i=1, i\neq j}^{3} \big(V_j(t-\xi) - V_i(t)\big) + \delta\, u_i(t) \Big), \\
\dot{m}_i(t) &= \alpha_m\big(V_i(t)\big)\big(1 - m_i(t)\big) - \beta_m\big(V_i(t)\big) m_i(t)\,, \\
\dot{h}_i(t) &= \alpha_h\big(V_i(t)\big)\big(1 - h_i(t)\big) - \beta_h\big(V_i(t)\big) h_i(t)\,, \\
\dot{n}_i(t) &= \alpha_n\big(V_i(t)\big)\big(1 - n_i(t)\big) - \beta_n\big(V_i(t)\big) n_i(t)\,, \qquad\qquad i = 1, 2, 3,
\end{aligned} \tag{3.1}$$

where the dot represents the derivative with respect to time t (measured in ms), V_i is the voltage of the i-th neuron (measured in mV), and the dimensionless quantities $m_i, h_i, n_i \in [0, 1]$ (called gating variables) characterize the 'openness' of the sodium and potassium ion channels embedded in the cell membrane. The conductances g_{Na}, g_{K}, g_{L} and the reference voltages V_{Na}, V_{K}, V_{L} for the sodium channels, potassium channels and the so-called 'leakage current' are given together with the membrane capacitance C and the driving current I in Appendix A by (A 1).

The term proportional to ε describes the electrotonic coupling between neurons. The conductance ε represents the coupling strength and ξ is the transmission delay described above. The term proportional to δ represents the control signal. The coefficient δ is the magnitude of the injected current and $u_i(t)$ describes the time variation of the input such that it can take the discrete values $0, 1, 2$. We assume that both the coupling and the input are weak, that is, $\varepsilon, \delta \ll 1$, and that they are in the same order of magnitude, i.e., $\delta = \mathcal{O}(|V|\varepsilon)$. For the parameters considered we have $|V| \approx 100$ and here we set $\delta = 250\,\varepsilon$. The equations for m_i, h_i, n_i are based on measurements and the nonlinear functions $\alpha_m(V)$, $\alpha_h(V)$, $\alpha_n(V)$, $\beta_m(V)$, $\beta_h(V)$, $\beta_n(V)$ are given in Appendix A by (A 2).

First, we describe the dynamics without inputs ($\delta = 0$) when varying the coupling strength ε and the coupling delay ξ. For $\varepsilon = 0$ the neurons are uncoupled and spike periodically (with period $T_{\mathrm{p}} \approx 10.43$). For small $\varepsilon > 0$ the qualitative shape of oscillations do not change but different cluster states can arise through the electronic interactions. In particular, three different patterns may exist: full synchrony (when all three neurons spike together); splay state (when no neurons spike together); and 1:2 state (when only two neurons spike together). These patterns correspond to the S_3 permutational symmetry in the system (interchangeability of neurons for $\delta = 0$) and these may be found by numerical simulation. Fig. 6 shows the simulation results for parameters $\xi = 5.5, \varepsilon = 0.03$ where all cluster states are stable: it depends on the initial conditions which state emerges. (The initial conditions are again chosen to be constant functions in the delay interval $t \in [-\xi, 0]$.) Notice that spikes are evenly spaced in the splay state in correspondence to the S_3 permutational symmetry. In the 1:2 state the phase difference between the pair and the singleton depends on the parameters and generally spikes are not evenly spaced. We remark that there are always two different splay states (distinguished by the order of spikes) and three different 1:2 states (distinguished by which oscillator is the singleton). For more details on clustering in globally coupled neural systems see (Brown *et al.* [2003]; Coombes [2008]; Orosz *et al.* [2009*b*]).

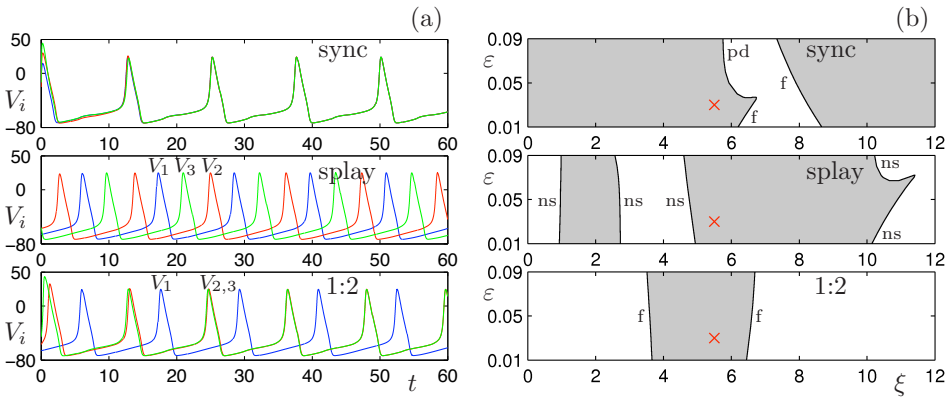

Figure 6. Different neural clusterings are shown in panel (a) and the related (ξ, ε) stability charts are displayed in panel (b). The shaded domains indicate stability and f, pd and ns denote fold, period doubling, and Neimark-Sacker bifurcations. The $\times$-s at $\xi = 5.5, \varepsilon = 0.3$ in panel (b) correspond to the parameters used in panel (a).

The different cluster states correspond to periodic orbits in phase space and one needs to use Floquet theory to determine their stability. In particular, the eigenvalues of the solution operator of (3.1) at T_p, the so-called Floquet multipliers, need to be calculated. A periodic motion is stable if all the infinitely many multipliers are located inside the unit circle in the complex plane. When varying the parameters stability losses may occur via fold bifurcation (when a real multiplier crosses the unit circle at $+1$), via period doubling bifurcation (when a real multiplier crosses the unit circle at -1), and via Neimark-Sacker bifurcation (when a pair of complex conjugate multipliers crosses the unit circle). Different periodic and quasiperiodic oscillations may arise through these bifurcations that are not discussed here in detail.

It is not possible to determine the stability boundaries in parameter space analytically but there exist numerical methods to perform this task. We use numerical continuation techniques, in particular the package DDE-Biftool, that allow us to follow branches of oscillatory solutions (both stable and unstable) as a function of parameters and detect the above bifurcation (Roose & Szalai [2007]). In order to determine the stability, the solution operator is discretized and represented by a large matrix whose eigenvalues approximate the Floquet multipliers. We remark that for large numbers of neurons one may apply semi-analytical methods to determine the stability for specific cluster states (e.g., the synchronized state and the splay state); see (Coombes [2008]).

We varied the delay parameter ξ and detected the above bifurcations for several different values of ε and the results are shown in the stability charts in Fig. 6(b). Shading indicates stability, the fold, period doubling and Neimark-Sacker bifurcations are denoted by f, pd and ns, respectively, and the $\times$-s correspond to the parameter values $\xi = 5.5, \varepsilon = 0.03$ used in Fig. 6(a). The 'sharp edges' along the stability boundaries correspond to codimension-two bifurcations, for example, the synchronized state undergoes a fold-period doubling bifurcation and the splay state undergoes a double Neimark-Sacker bifurcation. The dynamics is potentially complex around such points. Furthermore, in certain regimes multiple unstable so-

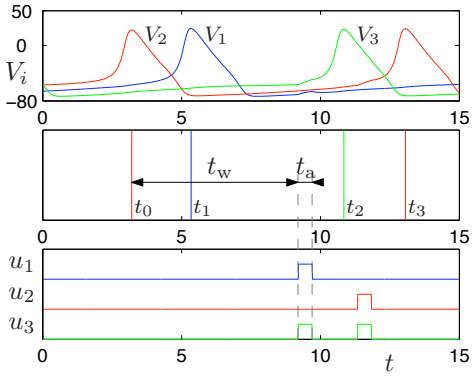

Figure 7. The event-based act-and-wait control algorithm: after a neuron spikes the controller 'waits' t_w time and then 'acts' for t_a time by injecting constant inputs to the other two neurons; see (3.2). Notice that $t_a \ll t_w$. From top to bottom: the voltage oscillations; the recorded spike times; the input signals.

lutions coexist with the stable solutions and the stable manifolds of the unstable solutions separate the regions of attractions of the stable solutions in state space. Unfolding these complexities is beyond the scope of this paper.

By studying the stability diagrams one may observe the qualitative changes of emergent dynamics as the time delay increases. For small delays (including zero delay) only the synchronous state is stable. This is followed by different domains of mono-, bi- and tristability. That is, by varying the time delay different cluster states may be realized.

Indeed, it is not possible to tune the natural delays in the system. However, the controller may inject external signals that mimic the effects of delayed coupling. To this end we construct an event-based act-and-wait controller (Danzl & Moehlis [2007]; Insperger [2006]) as follows. We record the event when a neuron spikes and after time t_w a constant signal of length t_a is injected to the other two neurons. The time intervals t_w and t_a are called the 'wait time' and the 'act time', respectively. Considering the initial condition $u_i(0) = 0$, $i = 1, 2, 3$, the control rules can be formalized as follows.

$$\begin{aligned} &\text{If neuron } i \text{ spikes at } t = t_0 \text{ then} \\ &u_j^+(t_0 + t_w) = u_j^-(t_0 + t_w) + 1 \\ &u_j^+(t_0 + t_w + t_a) = u_j^-(t_0 + t_w + t_a) - 1 \\ &\text{for all } j \neq i. \end{aligned} \tag{3.2}$$

This algorithm is demonstrated in Fig. 7. Recall that $u_i(t)$ can only take the discrete values $0, 1, 2$ such that $u_i(t) = 2$ occurs if at least two neurons spiked within a time interval of t_a. In order to obtain 'spiky' inputs we consider $t_a \ll t_w$. In particular, we fix the act time at $t_a = 0.5$ and vary the wait time t_w.

We define a scalar observable, called the order parameter, to quantify the emergent state of the system:

$$R = \frac{1}{3}\left| e^{i\,2\pi\frac{t_1 - t_0}{t_3 - t_0}} + e^{i\,2\pi\frac{t_2 - t_0}{t_3 - t_0}} + e^{i\,2\pi} \right|. \tag{3.3}$$

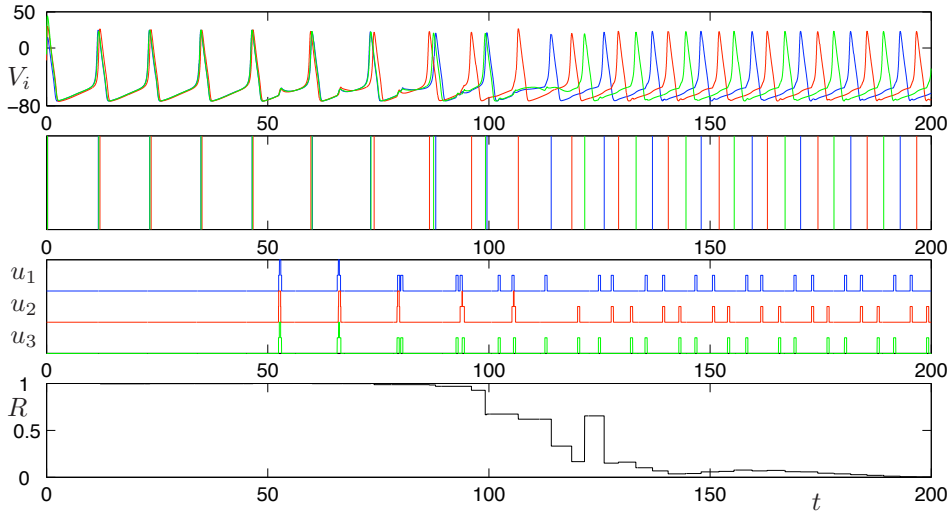

Figure 8. Driving the system from full synchrony to a splay state with the controller for $\xi = 0$, $\varepsilon = 0.06$ and $t_{\rm w} = 6.0$. From top to bottom: the voltage oscillations; the recorded spike times; the input signals; the order parameter (3.3).

This represents the phase relation of the last four spikes arrived at $t_0 \leq t_1 \leq t_2 \leq t_3$, such that the spikes at t_0 and t_3 were produced by the same neuron while the spikes at t_1 and t_2 were produced by the other two neurons; see Fig .7. This quantity has to be updated when a new spike arrives at t_4 according to the update rule $t_0 \leftarrow t_1$, $t_1 \leftarrow t_2$, $t_2 \leftarrow t_3$, $t_3 \leftarrow t_4$. In fact, R is an 'event-based version' of the order parameter used in phase oscillator networks where the phase information is continuously available (Strogatz [2000]). Notice that $R = 1$ for the fully synchronous state and $R = 0$ for the splay state (with evenly spaced spikes). For the 1:2 state (with general phase difference between the singleton and the pair) we have $1/3 \leq R < 1$ such that the minimum $R = 1/3$ is reached when the spikes are evenly spaced.

In Fig. 8 the controller's action is shown for parameters $\xi = 0, \varepsilon = 0.06$. One may observe that without inputs ($t \lesssim 50$) the system approaches the fully synchronous state since that is the only stable state for these parameters; see Fig. 6(b). After each neuron has spiked five times the controller is switched on using $t_{\rm w} = 6.0$. (Notice that for $\xi = 6.0, \varepsilon = 0.06$ the synchronous state is unstable in Fig. 6(b)). The controller drives the system away from the fully synchronous state into a splay state as shown in the top two panels in Fig. 8. The changes in the spatiotemporal pattern of inputs and the time evolution of the order parameter R (that goes from 1 to 0) are displayed it the bottom panels.

In order to test the robustness of the proposed algorithm we vary the wait time $t_{\rm w}$ and the coupling strength ε (for zero coupling delay $\xi = 0$) and read the asymptotic value of the order parameter (taken at $t = 1000$). The shading of the $(t_{\rm w}, \varepsilon)$-plane in Fig. 9 represents the value of R such that white corresponds to $R = 0$ (splay state) while the darkest tone corresponds to $R = 1$ (synchronized state). Notice the well pronounced boundaries between regions of qualitatively different

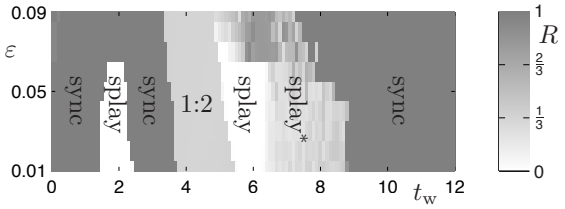

Figure 9. The asymptotic value of the order parameter R is depicted by shading in the (t_w, ε)-plane for $\xi = 0$; see the colorbar on the right. The states approached are written in each regime. The splay* state is a splay-like state where the spikes are not evenly spaced.

behaviors. We remark that for the 1:2 state $R \approx 1/3$ meaning that spikes are almost evenly spaced. In the splay* regime a splay-like state emerges such that the spikes are not evenly spaced. Such state may exist since the inputs destroy the S_3 permutation symmetry for $\delta > 0$. In the splay* state the order parameter does not approach a particular value but keeps oscillating, resulting in the 'granular' shading in this regime. The good match between the location of certain patterns in Fig. 9 and Fig. 6(b) justifies the idea of the controller: the waiting time t_w can serve as an effective time delay.

Notice that for larger values of ε the splay regimes become smaller which may be compensated by slightly increasing the input magnitude δ. Choosing different initial conditions in the bi- and tristable regimes in Fig. 6(b) the emergent states may differ from those in Fig. 9. For example, for certain initial conditions the synchrony may not be destroyed for $t_w \approx 2$, but it always disappears for $t_w \approx 6$.

4. Conclusions and discussion

In this paper we demonstrated that designing time delays is an efficient tool for controlling the behavior of complex biological networks. By varying the delays one may 'set the timing' of the control signals and so stabilize unstable equilibria or unstable oscillations. Thus, one may succeed with the control design even when strong constraints are imposed on the gains and on the qualitative features of the input (that would impede stabilizations for zero delay). We demonstrated this strategy in a gene regulatory network and in a neural network by driving the systems away from potentially harmful oscillatory behavior either to an equilibrium or to a chosen rhythmic cluster state. We achieved this by applying bio-compatible inputs.

The considered networks were extremely simple since these were chosen to serve as demonstrative examples. It will be necessary to repeat the calculations for more realistic setups (e.g., larger networks) in order to test the robustness of the proposed algorithms. Ultimately, the controllers also need to be validated by experiments. Nevertheless, we firmly believe that the methodology presented in this paper can be applied to a wide range of biological systems where delays, instead of causing undesired oscillations, can stabilize desired states.

Appendix A. Parameters for the Hodgkin-Huxley model

Here we define the parameters

$$\begin{aligned} g_{\mathrm{Na}} &= 120\,[\mathrm{mS/cm^2}]\,, & V_{\mathrm{Na}} &= 50\,[\mathrm{mV}]\,,\\ g_{\mathrm{K}} &= 36\,[\mathrm{mS/cm^2}]\,, & V_{\mathrm{K}} &= -77\,[\mathrm{mV}]\,,\\ g_{\mathrm{L}} &= 0.3\,[\mathrm{mS/cm^2}]\,, & V_{\mathrm{L}} &= -54.4\,[\mathrm{mV}]\,,\\ I &= 20\,[\mu\mathrm{A/cm^2}]\,, & C &= 1\,[\mu\mathrm{F/cm^2}]\,, \end{aligned} \tag{A 1}$$

and the functions

$$\begin{aligned} \alpha_m(V) &= \tfrac{0.1\,(V+40)}{1-\mathrm{e}^{-\frac{V+40}{10}}}\,, & \beta_m(V) &= 4\,\mathrm{e}^{-\frac{V+65}{18}}\,,\\ \alpha_h(V) &= 0.07\,\mathrm{e}^{-\frac{V+65}{20}}\,, & \beta_h(V) &= \tfrac{1}{1+\mathrm{e}^{-\frac{V+35}{10}}}\,,\\ \alpha_n(V) &= \tfrac{0.01\,(V+55)}{1-\mathrm{e}^{-\frac{V+55}{10}}}\,, & \beta_n(V) &= 0.125\,\mathrm{e}^{-\frac{V+65}{80}}\,. \end{aligned} \tag{A 2}$$

used in the Hodgkin-Huxley model (3.1).

References

Åström, K. J. & Murray, R. M. 2008 *Feedback systems: An introduction for scientists and engineers*. Princeton University Press.

Bolouri, H. 2008 *Computational modeling of gene regulatory networks – a primer*. Imperial College Press.

Brown, E., Holmes, P. & Moehlis, J. 2003 Globally coupled oscillator networks. In *Perspectives and problems in nonlinear science: A celebratory volume in honor of Larry Sirovich* (eds E. Kaplan, J. E. Marsden & K. R. Sreenivasan), pp. 183–215. Springer.

Campbell, S. A. 2007 Time delays in neural systems. In *Handbook of brain connectivity* (eds V. K. Jirsa & A. R. McIntosh), Understanding Complex Systems, pp. 65–90. Springer.

Chalfie, M., Tu, Y., Euskirchen, G., Ward, W. W. & Prasher, D. C. 1994 Green fluorescent protein as a marker of gene-expression. *Science*, **263**(5148), 802–805.

Chen, L. & Aihara, K. 2002 Stability of genetic regulatory networks with time delay. *IEEE Transactions on circuits and systems I: Fundamental Theory and Applications*, **49**(5), 602–608.

Coombes, S. 2008 Neuronal network with gap junctions: a study of piecewise linear planar neuron models. *SIAM Journal on Applied Dynamical Systems*, **7**(3), 1101–1129.

Coombes, S. & Laing, C. 2009 Delays in activity-based neural networks. *Philosophical Transactions of The Royal Society A*, **367**(1891), 1117–1129.

Courey, A. J. 2008 *Mechanisms in transcriptional regulation*. Blackwell Publishing.

Cox, R. S., Surette, M. G. & Elowitz, M. B. 2007 Programming gene expression with combinatorial promoters. *Molecular Systems Biology*, **3**(145), 1–11.

Danzl, P. & Moehlis, J. 2007 Event-based feedback control of nonlinear oscillators using phase response curves. In *Proceedings of the 46th IEEE conference on decision and control*, pp. 5806–5811.

Dombovári, Z., Wilson, R. E. & Stépán, G. 2008 Estimates of the bistable region in metal cutting. *Proceedings of the Royal Society A*, **464**(2100), 3255–3271.

Dunlap, J. C. 1999 Molecular bases for circadian clocks. *Cell*, **96**(2), 271–290.

Elowitz, M. B. & Leibler, S. 2000 A synthetic oscillatory network of transcriptional regulators. *Nature*, **403**(6767), 335–338.

Ermentrout, B. & Ko, T.-W. 2009 Delays and weakly coupled neuronal oscillators. *Philosophical Transactions of The Royal Society A*, **367**(1891), 1097–1115.

Gardner, T. S., Cantor, C. R. & Collins, J. J. 2000 Construction of a genetic toggle switch in Escherichia coli. *Nature*, **403**(6767), 339–342.

Hodgkin, A. L. & Huxley, A. F. 1952 A quantitative description of membrane current and its application to conduction and excitation in nerve. *Journal of Physiology*, **117**(4), 500–544.

Insperger, T. 2006 Act-and-wait concept for continuous-time control systems with feedback delay. *IEEE Transactions on Control Systems Technology*, **14**(5), 974–977.

Kirst, C., Geisel, T. & Timme, M. 2009 Sequential desynchronization in networks of spiking neurons. *Physical Review Letters*, **102**(6), 068 101.

Mascolo, S. 1999 Congestion control in high-speed communication networks using the Smith principle. *Automatica*, **35**(12), 1921–1935.

Monk, N. A. M. 2003 Oscillatory expression of Hes1, p53, and NF-κB driven by transcriptional time delays. *Current Biology*, **13**(16), 1409–1413.

Novák, B. & Tyson, J. J. 2008 Design principles of biochemical oscillators. *Nature Reviews Molecular Cell Biology*, **9**(12), 981–991.

Olfati-Saber, R. & Murray, R. M. 2004 Consensus problems in networks of agents with switching topology and time-delays. *IEEE Transactions on Automatic Control*, **49**(9), 1520–1533.

Orosz, G., Ashwin, P. & Townley, S. 2009*a* Learning of spatio-temporal codes in a coupled oscillator system. *IEEE Transactions on Neural Networks*, **20**(7), 1135–1147.

Orosz, G., Moehlis, J. & Ashwin, P. 2009*b* Designing the dynamics of globally coupled oscillators. *Progress of Theoretical Physics*, **122**(3).

Popovych, O., Hauptmann, C. & Tass, P. A. 2006 Control of neuronal synchrony by nonlinear delayed feedback. *Biological Cybernetics*, **95**(1), 69–85.

Rabinovich, M. I., Varona, P., Selverston, A. I. & Abarbanel, H. D. I. 2006 Dynamical principles in neuroscience. *Reviews of Modern Physics*, **78**(4), 1213–1265.

Roose, D. & Szalai, R. 2007 Continuation and bifurcation analysis of delay differential equations. In *Numerical continuation methods for dynamical systems* (eds B. Krauskopf, H. M. Osinga & J. Galan-Vioque), Understanding Complex Systems, pp. 359–399. Springer.

Sarpeshkar, R., Wattanapanitch, W., Arfin, S. K., Rapoport, B. I., Mandal, S., Baker, M. W., Fee, M. S., Musallam, S. & Andersen, R. A. 2008 Low-power circuits for brain-machine interfaces. *IEEE Transactions on Biomedical Circuits and Systems*, **2**(3), 173–183.

Stépán, G. 1989 *Retarded dynamical systems: Stability and characteristic functions*, vol. 210 of *Pitman Research Notes in Mathematics*. Longman.

Stépán, G. 2001 Vibrations of machines subjected to digital force control. *International Journal of Solids and Structures*, **38**(10-13), 2149–2159.

Stricker, J., Cookson, S., Bennett, M. R., Mather, W. H., Tsimring, L. S. & Hasty, J. 2008 A fast, robust and tunable synthetic gene oscillator. *Nature*, **456**(7221), 516–U39.

Strogatz, S. H. 2000 From Kuramoto to Crawford: exploring the onset of synchronization in populations of coupled oscillators. *Physica D*, **143**(1-4), 1–20.

Ugander, J. 2008 Delay-dependent stability of genetic regulatory networks. Master's thesis, Department of Automatic Control, Lund University, Sweden. `https://www.control.lth.se/database/publications/article.pike?artkey=5819`.